Sensors & Diagnostics

PAPER

View Article Online
View Journal | View Issue

Cite this: *Sens. Diagn.*, 2024, **3**, 1167

Antibody fluorescein-doped silica nanobioconjugates for the ultrasensitive detection of prostate-specific antigen†

Tumelo Msutu,[a] Omotayo Adeniyi[a] and Philani Mashazi *[ab]

Herein, we report the bioconjugation of anti-prostate-specific antigen polyclonal antibodies (pAb) onto the fluorescein-doped silica nanoparticles to detect prostate-specific antigen (PSA). Fluorescein-isothiocyanate (FITC), a fluorescent dye, was reacted with (3-aminopropyl)triethoxysilane (APTES) to form the FITC-APTES organosilane precursor. FITC-APTES was mixed with tetraethoxysilane (TEOS) to form fluorescent silica nanoparticles (FITC@SiO_2NPs) containing 3% and 6% of dye loading. The silica nanoparticles prevented the dye from leaching and promoted the fluorescent signal amplification for the detection of PSA. Phenylboronic acid (PBA) was coated onto the fluorescent silica nanoparticles for the oriented antibody immobilization *via* the boronate ester to form FITC@SiO_2-PBA-pAb. The fluorescent silica nanobioconjugates exhibited an emission peak at 518 nm, which was stable over time. A fluorescence sandwich-type immunoassay was used for the detection of PSA using FITC@SiO_2-PBA-pAb. Alkaline hydrolysis of the sensing nanobioconjugates afforded enhanced sensitivity by releasing FITC molecules. In buffer samples, the fluorescent immunosensor exhibited a linear correlation range from 2.0 pg mL^{-1} to 50 ng mL^{-1}. The linear range was from 2.0 pg mL^{-1} to 100 ng mL^{-1} in newborn calf serum (representing real samples). The limit of detection (LOD) was 8.25 fg mL^{-1} with a limit of quantification (LOQ) of 27.2 fg mL^{-1} in PBS (pH 7.4) after NaOH dissolution. A fluorescence immunosensor was used to detect PSA in spiked newborn calf serum with NaOH dissolution. It exhibited an LOD value of 33.0 fg mL^{-1} and LOQ value of 0.109 pg mL^{-1}. The developed fluorescence immunosensor showed high selectivity and specificity for PSA. The detection of prostate-specific antigen in newborn calf serum samples exhibited no matrix interferences.

Received 15th April 2024,
Accepted 16th May 2024

DOI: 10.1039/d4sd00119b

rsc.li/sensors

1 Introduction

The emergence of prostate cancer (PCa) as the most frequently diagnosed malignant cancer continues to attract research interest. PCa is the second leading cause of cancer deaths among men[1] and the fifth leading cause of cancer-related deaths worldwide.[2,3] Prostate-specific antigen (PSA) is the biomarker used for the detection of prostate cancer and is reliable for early diagnosis, screening, prognosis, monitoring, and prostate cancer recurrence.[4–6] Clinical identification of PCa is measured as the total PSA, that is, a sum of both free and complex PSA found in the patient's serum or seminal fluid. The total PSA levels are significantly increased in the serum of prostate cancer patients between 2.5 ng mL^{-1} and 10 ng mL^{-1}.[7–9] This is due to cell mutation and over-secretion of PSA, leading to the cell membrane (a basal membrane) disruption, and the PSA leaking into the bloodstream.[10,11] There is therefore a need for the development of several clinical diagnostic systems for the detection and quantification of PSA that aim to improve PSA tests for the early detection of PCa.

Current methods for PSA detection include commercial enzyme-linked immunosorbent assays,[12,13] electrochemical immunosensors,[6,14] colorimetric immunoassays,[15,16] and dual-mode fluorescence immunosensors.[17] Colorimetric and electrochemical detection methods use antibodies labelled with enzymes such as horseradish peroxidase or alkaline phosphatase as the detection probe. However, enzymes denature over time and are not stable under extreme assay conditions (pH and temperature). Labelling antibodies with enzymes is a challenging and tedious process, and purification procedures of the enzyme–antibody conjugates reduce enzyme activity and sensitivity during immunoassay detection. The fluorescence immunosensor uses fluorophores

[a] *Department of Chemistry, Rhodes University, P.O. Box 94, Makhanda, 6140, South Africa. E-mail: p.mashazi@ru.ac.za*
[b] *Institute for Nanotechnology Innovation, Rhodes University, P.O. Box 94, Makhanda, 6140, South Africa*

† Electronic supplementary information (ESI) available: The materials, characterization and methods are further discussed in the ESI. See DOI: https://doi.org/10.1039/d4sd00119b

that sometimes undergo quenching when attached to the antibody through an energy transfer mechanism called Förster (fluorescence) resonance energy transfer (FRET).[17]

The research interest in fluorescence immunoassays has been increasing due to the use of fluorophores with high extinction coefficients for high sensitivity, low limits of detection, and ease of preparation at low cost.[18,19] Conventional fluorescence-based immunosensors use fluorophore-labelled antibodies, which contain quantum dots,[20–22] organic dyes,[23,24] and up-conversion nanoparticles.[25] The major challenge of using fluorophores is fluorescence quenching upon bioconjugation.[26–28] Encapsulation of fluorophores into nanostructures such as silica nanoparticles and liposomes has been reported to overcome these limitations.[29–32] In addition, dye overloading into the nanomaterials also results in fluorescence quenching,[29–34] due to the phenomenon called highest occupied molecular orbital-Förster resonance energy transfer (HOMO-FRET).[28–35] The potential solution for reducing HOMO-FRET is dissolution, which results in the fluorophores dissolving back into solution and thus allowing for their fluorescence. In this study, we investigated alkaline dissolution of fluorescein-doped silica nanoparticles using NaOH to release fluorophores. Dye loading at two percentages was investigated (3% and 6%) with the 6% representing an overloaded nanoparticles and to see the effect of dissolution on dye loading. This resulted in a fluorescence signal amplification and enhanced sensitive detection of PSA. Alkaline dissolution method was compared with the PSA detection using the intact fluorescein-doped silica nanoparticles. The preparation and characterization of the fluorescein-doped silica nanoparticles was conducted and bioconjugation with anti-PSA polyclonal antibodies (pAb) was confirmed. Anti-PSA antibodies (pAb) were immobilized in an oriented manner using phenylboronic acid functionalization for specific, selective and sensitive detection of PSA. Here, to the best of our knowledge, the use of silica nanoparticles doped with FITC for the detection of PSA is reported for the first time.

2 Materials and methods

2.1 Biological reagents

The polyclonal (pAb) sheep anti-human prostate-specific antibody (7820-0154), monoclonal (mAb) mouse anti-human prostate-specific antibody (7820-0370), and prostate-specific antigens (PSA) were purchased from Bio-rad Laboratory Ltd (USA). The serum samples were prepared using newborn calf serum purchased from Sigma-Aldrich (USA). All reagents and solvents in this study were of analytical grade and used as received from the supplier. Other reagents and methods are indicated in the ESI.† Ultra-pure water with a resistivity of 18 MΩ cm (at 25 °C) was obtained from a Milli-Q Water Purification System (Millipore Corp. Bedford, MA, USA) and was used for the preparations of aqueous solutions.

2.1.1 Bioconjugation of anti-PSA pAb onto FITC@SiO_2-PBANPs. The bioconjugation of anti-PSA pAb onto FITC@SiO_2-PBANPs was *via* boronate ester reaction with the antibody Fc-glycans. FITC@SiO_2-PBANPs (2.0 mg) were dispersed in cold PBS buffer (2.0 mL, pH 7.4, 10 mM) and stirred for 10 min. Polyclonal anti-PSA antibody (50 μL, 10 μg mL^{-1}) was added to the solution. The mixture was kept at 4 °C, continuously stirred slowly, and allowed to react for 6 hours. The unbound pAb was isolated from FITC@SiO_2-PBA-pAb using centrifugation and washing with 4 °C cold PBS buffer (pH 7.4). The unreacted boronic acid sites were blocked by incubating FITC@SiO_2-PBA-pAbNPs in 4 °C cold PBS (pH 7.4, 10 mM) containing D-glucose solution (50.0 μg mL^{-1}, 60.0 mg, 0.33 mmol). After 2 hours, FITC@SiO_2-PBA-pAb/glucose nanoparticles were formed, which were washed three times with 4 °C cold PBS buffer (pH 7.4, 10 mM). FITC@SiO_2-PBA-pAb/glucose nanoparticles were suspended in PBS buffer (2.0 mL, pH 7.4, 10 mM) and kept at 4 °C before use. FTIR [(ATR), τ_{max}/cm^{-1}]: 3348 (N–H), 1639 (amide I), and 1322 (B–O). UV-vis [λ (nm), log(ε)]: 495 (3.8). The Bradford assay was used to determine the amount pAb that was bioconjugated onto FITC-doped silica nanoparticles. The experimental conditions are outlined in the ESI.†

2.2 Capture and detection of PSA, Scheme 1

Sandwich immunoassay detection of PSA following three steps:

(i) Attachment of anti-PSA monoclonal antibodies (mAbs) as captured on the microplate and blocking of non-specific binding sites with BSA.

(ii) Capture of the PSA (changes in PSA concentrations investigated), and

(iii) Detection of the captured PSA with FITC@SiO_2-PBA-pAb/glucose nanoparticles.

2.2.1 Attachment of capture anti-PSA monoclonal antibody (mAb), Scheme 1(a). Black Nuc 96 microwell plates were used for PSA sensing. For the positive control wells, mAb (200 μL, 10.0 μg mL^{-1}) diluted in sodium-bicarbonate buffer (10 mM, pH 9.5) was added into the microwells, and incubated for 12 hours at 4 °C. This resulted in the attachment of mAb onto the microwell, represented as well/mAb. The modified wells were washed three times with washing buffer (PBST, 10 mM, pH 7.4) to remove loosely bound mAb. Non-specific binding sites on the microwells were blocked with PBST blocking buffer (300 μL, pH 7.4, 10 mM) containing 2% BSA and incubated at room temperature for 3 hours, represented as well/mAb/BSA after washing three times with 4 °C PBST (pH 7.4) followed by a final rinse with PBS (pH 7.4). The negative control wells were modified with only 2% BSA in PBST blocking buffer (300 μL, pH 7.4) and washed three times to remove the loosely bound BSA to form well/BSA.

2.2.2 Detection of PSA using FITC@SiO_2-PBA-pAb/glucose, Scheme 1(a). A sandwich immunoassay protocol was used for PSA detection. PSA (200 μL) of varying concentrations was added to the well/mAb/BSA and incubated to yield well/mAb

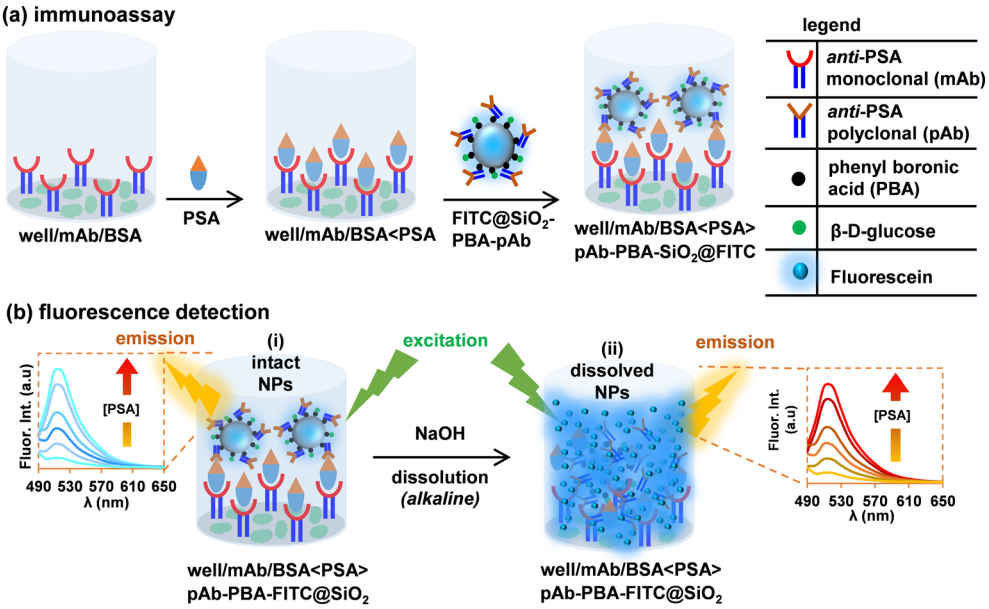

Scheme 1 Capture of PSA on the well/mAb/BSA, and sensing with FITC@SiO_2-PBA-pAb fluorescence nanobioconjugates.

> PSA. After 2 h, the microplate wells were washed 3 times with 4 °C cold PBS (pH 7.4, 10 mM) to remove unbound PSA. The nanobioconjugate solution (FITC@SiO_2-PBA-pAb/glucose, 200 μL, 200 μg mL^{-1}) was added to the wells. The wells were incubated for 50 min at room temperature, to yield the sandwich immunoassay. The wells were washed three times with PBST (pH 7.4, 10 mM) to remove unbounded nanobioconjugates. The fluorescence signal was measured for:

(i) intact nanobioconjugates captured, as demonstrated in Scheme 1(b)(i), and

(ii) NaOH (200 μL, 10 mM) alkaline solution was used to dissolve the silica shell and released FITC molecules, as demonstrated in Scheme 1(b)(ii).

The negative wells were treated the same way as the positive wells except only the BSA was coated. In the negative control wells, no PSA capture was expected and subsequently there was no capture of FITC@SiO_2-PBA-pAb/glucose.

3 Results and discussion

3.1 Preparation of FITC@SiO_2-PBA-pAb/glucose

The successful preparation of fluorescein-doped silica nanobioconjugates involved the steps shown in Scheme S3 in the ESI.† The organosilane precursor was synthesized by covalent coupling of FITC (**1**) and APTES (**2**) *via* a thiourea linkage to form FITC-APTES (**3**), Scheme S1.† FITC-APTES (**3**) was encapsulated into silica nanoparticles to form fluorescein-doped silica nanoparticles, FITC@SiO_2NPs, *via* a quaternary water-in-oil micro-emulsion method. Different amounts of FITC-APTES (**3**) were added to tetraethoxysilane (TEOS) to obtain different loadings into the fluorescein-doped silica nanoparticles in the ammonium hydroxide (NH_4OH) solution. The phenylboronic acid functionalized FITC@SiO_2NPs resulted from modification with triethoxysilane-propyl-3-amido phenylboronic acid (TES-PBA (**5**), Scheme S2†) to form FITC@SiO_2-PBANPs also in the ammonium hydroxide solution. The successful bioconjugation with pAbs and non-specific binding sites blocked with D-glucose resulted in the formation of FITC@SiO_2-PBA-pAb/glucose. The effect of dye-loading into silica nanoparticles plays a crucial role in the high sensitivity of fluorescent nanobioconjugates for ultra-low detection of biomarkers.[34,36,37] Here, we prepared, characterized and evaluated their fluorescence properties of 3.0% and 6.0% FITC@SiO_2NPs. After bioconjugation, the FITC@SiO_2NPs were used to fabricate simple, ultrasensitive fluorescence-linked immunosorbent assays (FLISA) for the detection of PSA.

3.2 Characterization of FITC@SiO_2-PBA-pAb/glucose

FT-IR spectrum shown in Fig. 1(a)(i) indicates the vibrational bands at 1036 cm^{-1}, 948 cm^{-1}, and 786 cm^{-1} due to asymmetric stretching of siloxane (Si–O–Si), (Si–O) groups, and silanol (Si–OH) groups, respectively. The presence of broad (O–H) peaks at 3287 cm^{-1} and small peaks exhibited at 1323 cm^{-1}, 1462 cm^{-1}, 1502 cm^{-1}, and 1642 cm^{-1} are due to the aromatic and aliphatic functional groups of FITC-APTES (**3**). The results confirmed the successful encapsulation of FITC-APTES (**3**) and the preparations of fluorescent silica nanoparticles, FITC-SiO_2NPs. FITC@SiO_2NPs were modified with TES-PBA (**5**) to form FITC@SiO_2-PBNPs. FT-IR spectrum shown in Fig. 1(a)(ii) indicated the presence of characteristic peaks at 3303 cm^{-1} corresponding to the O–H stretching of the phenylboronic acid, and the N–H bending from the TES-PBA (**5**) to the carbonyl oxygen of the phenylboronic acid. This was accompanied by the presence of a C=O stretch at

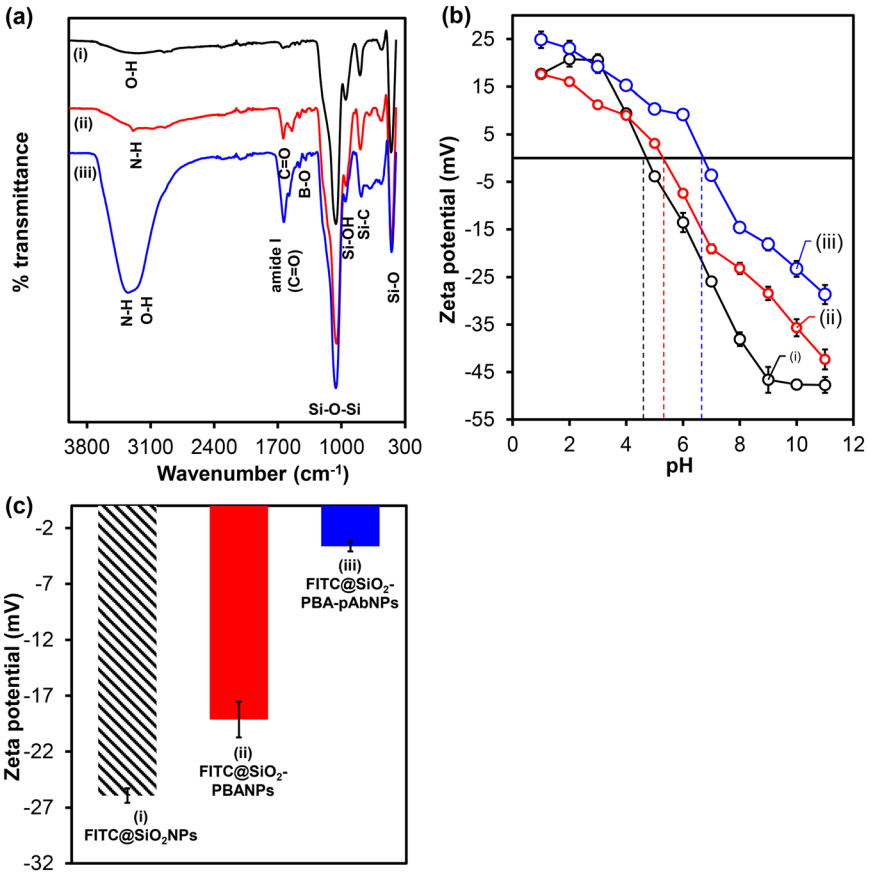

Fig. 1 (a) FTIR spectra, (b) zeta potential (mV) *vs.* pH, and (c) bar graph of zeta-potential at pH (7.0) of (i) FITC@SiO_2NPs, (ii) FITC@SiO_2-PBANPs, and (iii) FITC@SiO_2-PBA-pAb. The data in (b) and (c) were measured in triplicates (n = 3).

1647 cm^{-1} and the emergence of the B–O vibrational stretch at 1395 cm^{-1} from the phenylboronic acid. The bioconjugation of pAbs onto FITC@SiO_2-PBANPs proceeded *via* the boronate ester bonds that were formed between the cis-diol of the antibody glycan moieties on the Fc region of the antibody. The boronic acid bioconjugation route helps maintain the orientation of the antibody for enhanced antigen binding. Fig. 1(a)(iii) shows the FT-IR spectrum of the FITC@SiO_2-PBA-pAb/glucose. The FT-IR spectrum shows the appearance of an intense stretching vibration at 1639 cm^{-1}, assigned to the amide (I) from the peptides from the pAb antibody. The broad absorption peak at 3328 cm^{-1}, was assigned to the presence of the NH_2 functional groups from the antibody. The peak shifts of B–O at 1322 cm^{-1} confirm the successful bioconjugation of the antibody.

The zeta (ζ) potential of FITC@SiO_2NPs with TES-PBA (**5**) and pAb confirmed the functionalization. The study of the changes in the zeta potential at different pH values confirmed the surface modification and charge on the fluorescent silica nanobioconjugates. Fig. 1(b) and (c) show the zeta potential measurements (surface charges) of the fluorescent silica nanoparticles as a function of pH. Fig. 1(b) shows the zeta potential (mV) plot at different pH values (1–10) and Fig. 1(c) the bar graph of zeta potential at pH (7.0) of 6.0% w/w (i) FITC@SiO_2NPs, (ii) FITC@SiO_2-PBANPs, and (iii) FITC@SiO_2-PBA-pAb. From Fig. 1(b) and (c), the FITC-doped silica nanoparticles exhibited pH-dependent zeta potential values. The zeta potential of (i) FITC@SiO_2NPs shows that the nanoparticles have a negative charge at higher pH values. The isoelectric point (IEP) of FITC@SiO_2NPs was at pH 4.8. A zeta potential value at pH 7.0 was −25.9 mV due to the deprotonated hydroxyl (–OH) groups from the silica and FITC. For FITC@SiO_2-PBANPs, the isoelectric point shifted to pH 5.3 and at pH 7.0 the zeta potential was −19.1 mV. This decrease in the zeta potential from −25.9 mV for FITC@SiO_2-NPs to −19.1 mV for FITC@SiO_2-PBA confirmed the successful functionalization with phenylboronic acid. After bioconjugation with pAb, the isoelectric point was observed at pH 6.8. The zeta potential of FITC@SiO_2-PBA-pAb decreased further to −3.6 mV. The decrease in zeta potential was attributed to the binding of the pAb to the phenylboronic acid *via* boronate ester to form FITC@SiO_2-PBA-pAb. Bioconjugation of pAb did not occur in the absence of phenylboronic acid as the zeta potential remained −19.1 mV and similar to FITC@SiO_2-PBANPs above. The change in zeta potential at different pH solutions confirmed the preparations of the fluorescent FITC@SiO_2-PBA-pAb nanobioconjugates.

To further confirm the successful preparation of FITC@SiO_2NPs at different (%, w/w) of FITC-APTES (**3**) loading and the effects of surface modification with TES-PBA

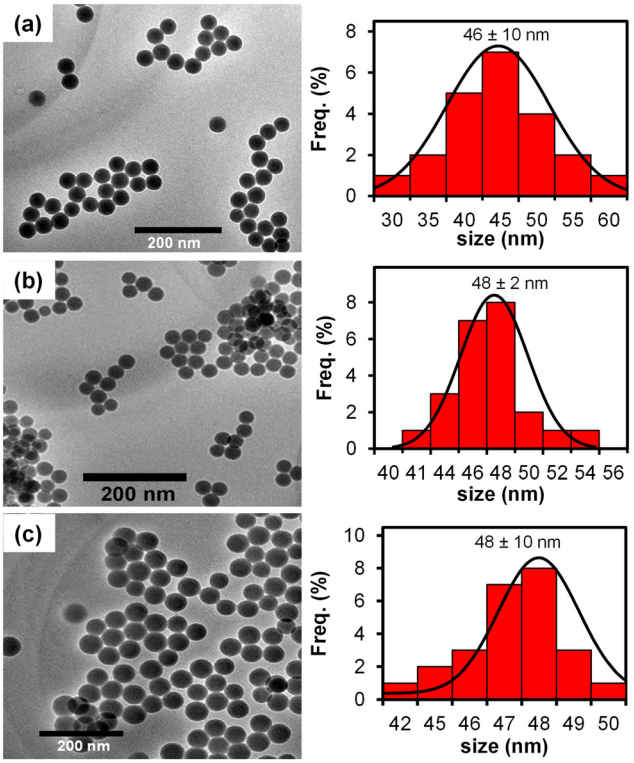

Fig. 2 TEM micrographs and corresponding histograms of 6% (a) FITC@SiO_2NPs, (b) FITC@SiO_2-PBANPs, and (c) FITC@SiO_2-PBA-pAb/glucose.

(5) TEM and EDS analysis were conducted. Fig. 2 shows the TEM micrographs and size distribution histograms of 6.0% (a) FITC@SiO_2NPs, (b) FITC@SiO_2-PBANPs and FITC@SiO_2-PBA-pAb/glucose. TEM micrographs of the nanoparticles were spherical and exhibited good monodispersity. For 6.0% loading, the average sizes were 46 ± 10 nm for FITC@SiO_2NPs shown in Fig. 2(a) and 48 ± 2 nm for FITC@SiO_2-PBANPs shown in Fig. 2(b). A 2 nm average size increase was observed after functionalization with phenylboronic acid to form FITC@SiO_2-PBANPs. The size distribution of FITC@SiO_2-PBA-pAb in Fig. 2(c) showed no size variation as compared to the FITC@SiO_2-PBANPs. This was due to the antibody being a protein molecule and under TEM measurement does not show the increase in the diameter. The average size distribution of 3.0% FITC@SiO_2NPs was 30 ± 3 nm, in Fig. S3(a).† An increase in the average size to 32 ± 2 nm for 3.0% FITC@SiO_2-PBANPs was observed after coating with phenylboronic acid in Fig. S3(b).† A 16 nm increase in the average size from 3.0% to 6.0% confirmed higher loading due to the increased concentration of FITC-APTES (**3**). In addition, the high concentration of FITC-APTES will result in high fluorescence. Other concentrations of FITC-APTES, which will result in lower than 3% or higher than 6%, will be investigated in future.

3.3 Bioconjugation with pAb to form FITC@SiO_2-PBA-pAb

The Bradford assay was used to monitor and quantify pAb bioconjugation onto FITC@SiO_2-PBANPs. UV-vis absorbance measurements at 595 nm corresponded to the BSA standard solutions and pAb. The concentration of pAb in the supernatant before and after bioconjugation gave the amount of pAb conjugated. The percentage conjugation efficiency (% CE) was calculated using eqn (1):

$$\%\ \mathrm{CE} = \frac{[\mathrm{pAb}]_0 - [\mathrm{pAb}]_f}{[\mathrm{pAb}]_0} \times 100 \quad (1)$$

where $[\mathrm{pAb}]_0$ and $[\mathrm{pAb}]_f$ indicate the initial and final concentrations of the pAb before and after bioconjugation, respectively. The % CE was found to be 79.3% corresponding to the amount of protein conjugated to form FITC@SiO_2-PBA-pAb/glucose nanobioprobe. The Bradford assay details are shown in Fig. S6† and confirmed the successful preparations of FITC@SiO_2-PBA-pAb/glucose nanobioconjugates.

3.4 Fluorescence analysis

3.4.1 Photophysical properties of fluorescein-silica nanobioconjugates. Fig. 3 shows the ground-state absorption and fluorescence emission spectra of (i) FITC (**1**), (ii) FITC-APTES (**3**), (iii) FITC@SiO_2NPs, (iv) FITC@SiO_2-PBANPs, and (v) FITC@SiO_2-PBA-pAb. In Fig. 3(i) and (ii), the UV-vis spectra exhibited a single absorption peak at 493 nm. The nanoparticles, FITC@SiO_2NPs, shown in Fig. 3(iii)–(v) exhibited a 2 nm shift with absorption peaks observed at 495 nm. A 2 nm shift was due to the interactions between FITC and APTES (**3**) in the silica nanoparticles matrix. The maximum fluorescence emission wavelength for FITC (**1**) was at 520 nm. The maximum fluorescence emission was at 518 nm for FITC-APTES (**3**) as shown in Fig. 3(ii) and FITC-doped silica nanoparticles, as shown in Fig. 3(iii)–(v). The fluorescence of FITC stayed intact even after the nanoparticle preparation and functionalization.

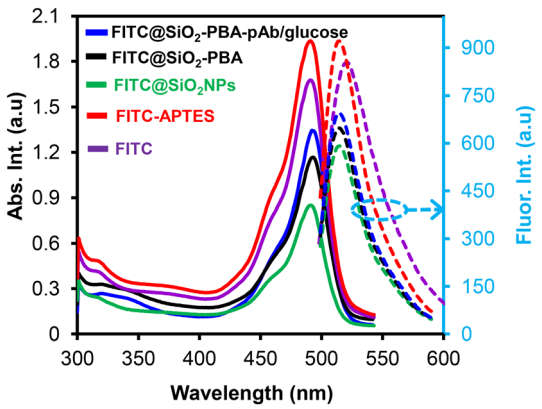

Fig. 3 Ground state absorption (solid lines) and fluorescence emission (dotted lines) spectra of FITC (**1**), FITC-APTES (**3**), FITC@SiO_2NPs, FITC@SiO_2-PBANPs, and FITC@SiO_2-PBA-pAb (the colours show reference to the materials).

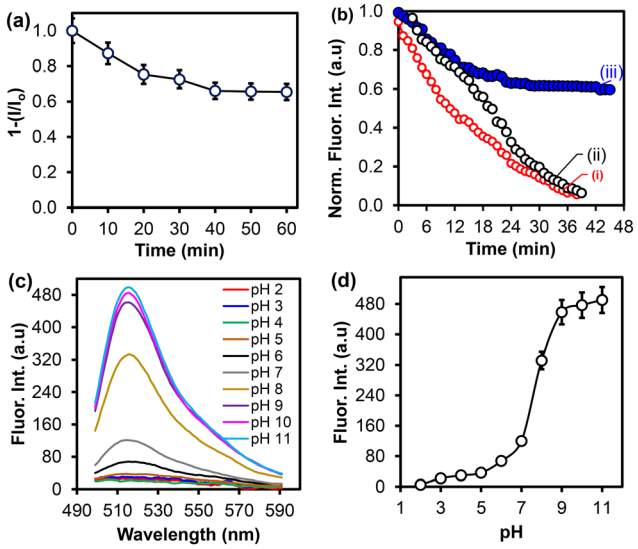

Fig. 4 Fluorescence intensity over time for (a) dye-leakage studies of FITC@SiO_2NPs, (b) photostability studies of (i) FITC (**1**), (ii) FITC-APTES (**2**), and (iii) FITC@SiO_2NPs, (c) fluorescence spectra, and (d) corresponding fluorescence intensity of FITC@SiO_2NPs at varied pH (2.0–11.0) in PBS (10 mM).

3.4.2 Dye-leakage, photostability, and effects of pH studies. The fluorescent properties of the sensing nanobioconjugates were optimized to obtain an excellent analytical performance of the fluorescent immunosensors. Fig. 4 shows the normalized fluorescence intensity over time of (a) dye-leaking studies on FITC@SiO_2NPs, and (b) photostability studies of (i) FITC (**1**), (ii) FITC-APTES (**3**), and (iii) FITC@SiO_2NPs in aqueous media, (c) fluorescence spectra in varied PBS buffer (pH 2.0–9.0, 10 mM), and (d) the corresponding pH response curve of FITC@SiO_2NPs. The nanoparticles were subjected to sonication to assess for mechanical dye leakage and the supernatant was measured. 65% FITC dye was retained within the silica nanoparticles after sonication for over a period of 50 min, as shown in Fig. 4(a). Fig. 4(b)(i) shows a sharp decrease in intensity as FITC (**1**) was photobleaching and after 40 min only 10% fluorescence intensity was observed. The same was observed for FITC-APTES (**3**), as shown in Fig. 4(b)(ii). However, when FITC was doped into the silica nanoparticles, it showed excellent photobleaching stability with more than 60% fluorescence intensity retained after 40 min, as shown in Fig. 4(b)(iii). Fig. 4(c) and (d) show the evaluation of the effects of pH on the photostability of the FITC@SiO_2NPs and the optimum buffer pH for the dissolution of the sensing nanobioconjugates. The fluorescence intensity increased with increasing pH values from 5.0 to 9.0 in PBS (10 mM). A sharp increase in the fluorescence intensity was between pH 7.0 to pH 9.0. At higher pH values above pH 7.0, the fluorescent silica nanoparticle shell disintegrated releasing FITC (**1**).[38] A complete disintegration of FITC@SiO_2NPs was at pH 9.0. NaOH (10 mM, pH 12) was used as the dissolution buffer to release FITC (**1**) for enhanced fluorescence detection. The

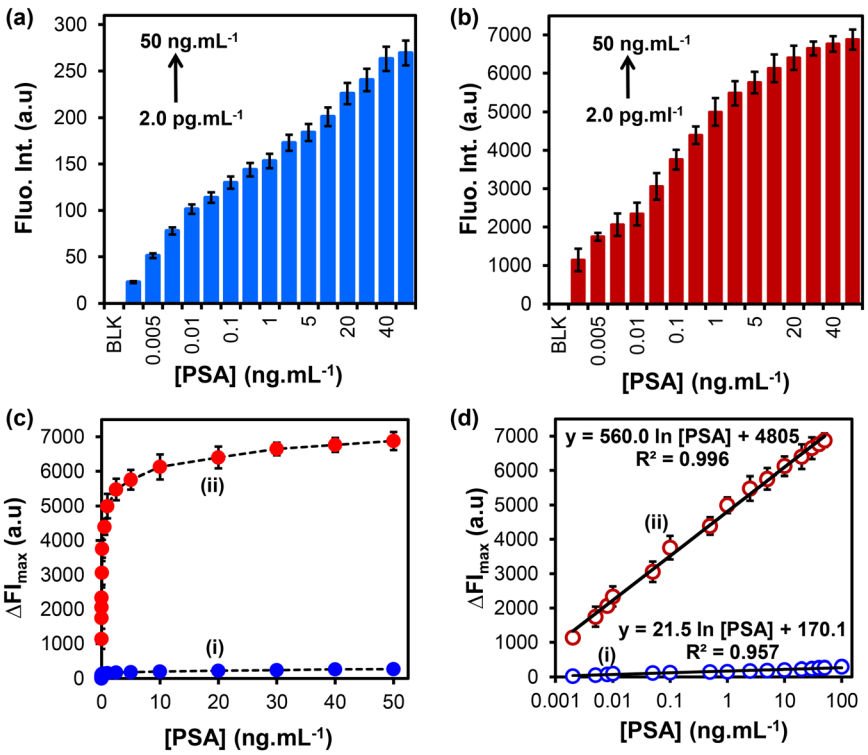

Fig. 5 Fluorescence emission of the FITC@SiO_2-PBA-pAb/glucose nanobioconjugates at increasing PSA concentrations from (2.0 pg mL^{-1}–100 ng mL^{-1}) (a) before and (b) after NaOH dissolution. (c) Dose–response curves and (d) calibration curve of relative fluorescence intensity (ΔFI_{max}) *vs.* [PSA] (i) before and (ii) after dissolution with NaOH (10 mM) (n = 3).

choice of NaOH is due to the dissolution of the silica matrix being accelerated at a higher pH and enhanced in the presence of cations such as sodium and potassium ions.[39]

3.5 Detection of PSA in buffer samples

The detection of PSA was achieved following the procedure shown in Scheme 1. Fig. 5(a) and (b) show the fluorescence emission spectra of FITC@SiO_2NPs nanobioconjugates detection at varied concentrations of PSA before and after the addition of NaOH (0.010 M), respectively. An increase in the fluorescence intensity was observed with increasing PSA concentrations from 2.0 pg mL^{-1} to 50 ng mL^{-1}. Dose–response curves of the changes in fluorescence intensity (ΔFI_{max}) against varied PSA concentrations were observed, as shown in Fig. 5(c). After NaOH dissolution, an increase in the fluorescence emission signal was observed due to the release of the encapsulated FITC fluorophores into the solution. The dissolution-based detection yielded a fluorescent intensity enhancement factor, which was higher when intact FITC@SiO_2NPs were used. The calibration curves of ΔFI_{max} against PSA concentrations in Fig. 5(d) show a linear relationship between the relative fluorescence intensity ($\Delta FI = FI_i - FI_o$) and PSA concentrations in the range of 2.0 pg mL^{-1} to 50 ng mL^{-1}. The semi-log plot with the concentration gave linear regression equations of both the intact eqn (2) and dissolution eqn (3) studies:

$$\Delta FI = 21.5 \ln[PSA] + 170.1 \quad (R^2 = 0.957) \tag{2}$$

$$\Delta FI = 560.0 \ln[PSA] - 4805 \quad (R^2 = 0.996) \tag{3}$$

The sensitivity for the intact nanobioconjugate detection was 21.5 (a.u) pg mL^{-1} and 560.0 (a.u) pg mL^{-1} after NaOH dissolution. A 26.4-fold increase after the dissolution of the fluorescein-doped silica nanobioconjugates was observed. The LOD and LOQ values were calculated according to the reported method,[40] LOD = $3S/b$ and LOQ = $10S/b$, where S is a standard deviation of the blank response and b is a slope of the calibration curve. For intact nanoparticles, the LOD was 0.37 pg mL^{-1} and LOQ was 1.22 pg mL^{-1}. After NaOH dissolution, the LOD was 8.25 fg mL^{-1} and the LOQ was 27.2 fg mL^{-1}. The LOD was approximately 5-fold lower in the dissolution studies. Therefore, the dissolution route resulted in a higher sensitivity attributed to the release of the FITC into the solution and the amplification of the emission fluorescence signals for ultrasensitive detection of PSA.

3.6 PSA detection in serum samples

We investigated the applicability of the fluorescent immunosensor in spiked newborn calf serum samples. The dissolution fluorescence-linked immunosorbent assay method was employed for the detection of PSA due to its enhanced signal. The serum samples were diluted 10-fold with PBS buffer pH (7.4) and spiked with known concentrations of PSA ranging from 2.0 pg mL^{-1} to 100 ng mL^{-1}. Serum samples without the addition of PSA were used as negative controls to confirm the non-specific binding of proteins in the serum. Fig. 6(a) shows that the fluorescence emission intensity increased with an increase in PSA concentrations spiked in the newborn calf serum. The average fluorescent signal of the negative controls was 128 ± 5.3 a.u (n = 3) and the intensity with the lowest concentrations of PSA (2.0 pg mL^{-1}) was 1202 ± 43.4 a.u (n = 3). This indicated that the proposed method could discriminate between positive and negative sera samples at low concentrations of PSA. An increase in the fluorescence emission intensity relative to the increase in PSA concentration is shown in Fig. 6(b). The calibration curve of the change in the fluorescent intensity ($\Delta FI = FI_i - FI_o$) *vs.* [PSA] was linear between 2.0 pg mL^{-1} to 100 ng mL^{-1}. A linear regression equation on a semi-log plot and the linear regression coefficient (R^2) are shown in eqn (4).

$$\Delta FI = 478.2 \ln[PSA] + 4503.2 \quad R^2 = 0.992 \tag{4}$$

The LOD and LOQ in newborn calf serum were calculated following a similar method as reported above. The linear concentration range of PSA detection was from 2.0 pg mL^{-1}

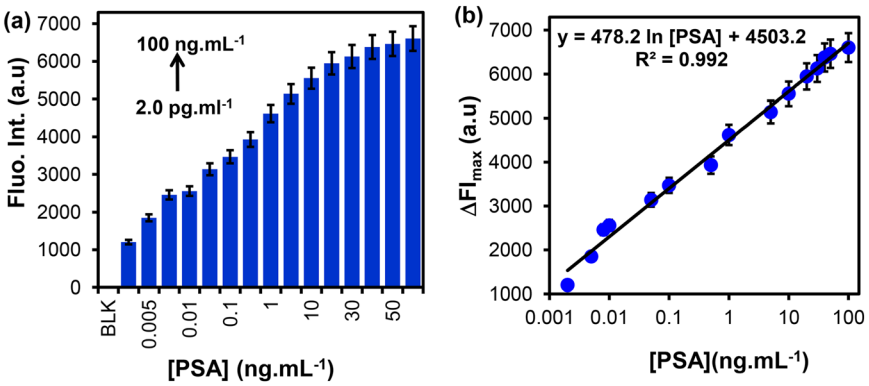

Fig. 6 (a) Fluorescence emissions for different concentrations of PSA (2.0 pg mL^{-1}–100 ng mL^{-1}), (b) calibration curve of relative fluorescence intensity (ΔFI) against [PSA] in the spiked new-born calf serum (2.0–100 ng mL^{-1}) (n = 3).

Table 1 A comparison of different analytical biosensors' performance for the detection of PSA

Detection probe	Signal monitored	Linear concentration range (LCR)	LOD	Ref.
FITC@SiO_2-PBA-pAb/glucose	Fluorescence (serum) (dissolution)	2.0 pg mL^{-1}–100 ng mL^{-1}	33.0 fg mL^{-1}	[TW]
	Fluorescence (buffer) (intact NPs)	2.0 pg mL^{-1}–50 ng mL^{-1}	0.37 pg mL^{-1}	[TW]
	Fluorescence (buffer) (dissolution)	2.0 pg mL^{-1}–50 ng mL^{-1}	8.25 fg mL^{-1}	[TW]
Multi-CAT-AuNPs-Ab_2	Colorimetric	50 pg mL^{-1}–20 ng mL^{-1}	30 pg mL^{-1}	41
HRP-Ab_2-SiO_2NSs	Fluorescence	30 pg mL^{-1}–100 ng mL^{-1}	10 pg mL^{-1}	42
CdTe@SiO_2	Fluorescence	10 pg mL^{-1}–5.0 ng mL^{-1}	3.0 pg mL^{-1}	43
rGO-Ca:CdSe-Ab_2	Photoelectrochemistry	5.0 pg mL^{-1}–50 ng mL^{-1}	2.6 pg mL^{-1}	44
GENLs-anti-PSA-pAb	Colorimetric (HRP)	0.10 pg mL^{-1}–100 mg mL^{-1}	53 fg mL^{-1}	45

TW: this work; Multi-CAT-AuNP-Ab_2: polyclonal goat anti-human PSA/catalase-labelled gold nanoparticles; HRP-Ab_2-SiO_2NSs: horseradish peroxidase-labelled monoclonal anti-PSA antibody/silicon dioxide nanospheres; CdTe@SiO_2-Ab_2: PSA-labelled cadmium telluride@silica core–shell nanoparticles; rGO-Ca:CdSe-Ab_2: cadmium selenide doped (CdSe) on the conducting framework of reduced graphene oxide; GENLs-anti-PSA-pAb: polyclonal sheep anti-human PSA/glucose encapsulated nanoliposomes.

to 100 ng mL^{-1}. The fluorescence immunosensor LOD was calculated to be 33.0 fg mL^{-1} and LOQ was 0.109 pg mL^{-1} (n = 3). The linear range and LOD of the proposed fluorescence-linked immunosorbent assay (FLISA) dissolution method of detection for PSA were compared between the serum samples and PSA buffer solutions, along with previously reported methods of detection for PSA, as summarized in Table 1. Previously reported methods using different detection methods gave LOD values of 30 pg mL^{-1} using Mutli-CAT-AuNPs-Ab_2,[41] 10 pg mL^{-1} using HRP-Ab_2-SiO_2NSs,[42] 3.0 pg mL^{-1} using CdTe@SiO_2-Ab_2,[43] and 2.6 pg mL^{-1} using rGO-Ca:CdSe-Ab_2.[44] The proposed FLISA immunosensor with NaOH dissolution gave a lower LOD of 8.25 fg mL^{-1} for PSA detection in buffer samples and LOD of 33.0 fg mL^{-1} in newborn calf serum. When compared to the LOD by Mwanza *et al.*,[45] which was 53 fg mL^{-1}, the proposed FLISA exhibited low LODs for the detection of PSA. The study employed a detection probe of GENLs-anti-PSA-pAb. However, as compared to other studies, the proposed FLISA offered several advantages, such as (i) simple preparation of highly fluorescent nanoparticles, (ii) photostable FITC in the silica nanoparticle, and (iii) amplified fluorescence signals after alkaline (NaOH) dissolution. Compared to the GENLs detection nanobioconjugates, fluorescein-doped silica nanobioconjugate followed a simple preparation route.

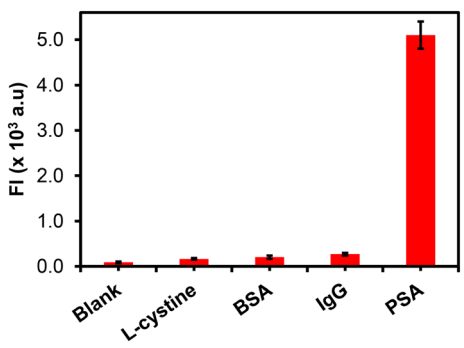

Fig. 7 The specificity studies of the fluorescent immunoassay for the detection of PSA and other analytes (L-cysteine, BSA, and IgG) (n = 3).

3.7 Selectivity and specificity for PSA detection

The specificity of the FLISA was investigated by determining the assay responses to other interfering analytes. The newborn calf serum in PBS solution was measured as prepared (blank) and after spiking with 50 ng mL^{-1} concentration of L-cysteine, BSA, IgG, and 20 ng mL^{-1} for PSA, as shown in Fig. 7. From Fig. 7, the study showed that only PSA-spiked newborn calf serum samples gave a significant fluorescence response signal as compared to other analytes, demonstrating the excellent specificity and selectivity of the immunosensor for PSA detection.

4 Conclusions

We developed a simple method for rapid and highly sensitive detection of PSA using anti-PSA polyclonal antibody fluorescent silica nanobioconjugates for fluorescence sensing. The step-by-step preparation and characterization of antibody-fluorescence silica nanoparticle nanobioconjugates was followed using microscopic and spectroscopic techniques. The preparation was successful as spherical and monodispersed fluorescence-antibody nanobioconjugates were obtained with 3% and 6% fluorescence dye loadings. The fluorescent silica nanobioconjugates exhibited excellent stability except under alkaline conditions used for enhanced PSA detection. Surface functionalization with boronic acid allowed for the oriented bioconjugation of anti-PSA-pAb, with glycan moiety on the Fc region. 6.0% Fluorescein-doped nanoparticles exhibited excellent and high fluorescence signals due to the high loading of fluorescein. The oriented pAb bioconjugation promoted specificity and selectivity for PSA antigens and other biomolecules were not detected even at higher concentrations. The dissolution of the FITC@SiO_2-PBA-pAb/glucose using NaOH resulted in amplified fluorescence signals. The combined effect of the low background noise and increased fluorescence intensity resulted in low detection limits and limit of quantification in fg mL^{-1} and pg mL^{-1}. The immunoassay in newborn calf serum samples further confirmed the excellent selectivity and specificity towards the detection of PSA, thus paving the way toward early detection and diagnosis of prostate cancer.

Data availability

Data will be made available on request.

Author contributions

Tumelo Msutu: conceptualization, methodology, formal analysis, validation, data curation, investigation, writing original draft, visualization. Omotayo Adeniyi: methodology, formal analysis, investigation. Philani Mashazi: conceptualization, methodology, validation, data curation, visualization, supervision, writing-review and editing, resources, project administration, funding acquisition.

Conflicts of interest

The authors declare no competing financial interest.

Acknowledgements

The National Research Foundation (NRF) through NRF-STINT Bilateral (UID 118725) and NRF CPRR Grant supported this work. Rhodes University through Researcher Development Grant (RDG P5/17/2015), Rated Research Grant (RRG) and Sandisa Imbewu. TM thanks Gauteng City Regional Academy (GCRA) for an MSc Scholarship.

References

1 S. K. Bechis, P. R. Carroll and M. R. Cooperberg, Impact of age at diagnosis on prostate cancer treatment and survival, *J. Clin. Oncol.*, 2011, **29**, 235–241.
2 C. Mattiuzzi and G. Lippi, Current Cancer Epidemiology, *J. Epidemiol. Glob. Health*, 2019, **9**, 217–222.
3 P. Rawla, Epidemiology of Prostate Cancer, *World J. Oncol.*, 2019, **10**, 63–89.
4 U.-H. Stenman, J. Leinonen, W.-M. Zhang and P. Finne, Prostate-specific antigen, *Semin. Cancer Biol.*, 1999, **9**, 83–93.
5 T. J. Polascik, J. E. Oesterling and A. W. Partin, Prostate specific antigen: A decade of discovery-what we have learned and where we are going, *J. Urol.*, 1999, **162**, 293–306.
6 N. V. Panini, G. A. Messina, E. Salinas, H. Fernández and J. Raba, Integrated microfluidic systems with an immunosensor modified with carbon nanotubes for detection of prostate specific antigen (PSA) in human serum samples, *Biosens. Bioelectron.*, 2008, **23**, 1145–1151.
7 E. A. Stura, B. H. Muller, M. Bossus, S. Michel, C. Jolivet-Reynaud and F. Ducancel, Crystal Structure of Human Prostate-Specific Antigen in a Sandwich Antibody Complex, *J. Mol. Biol.*, 2011, **414**, 530–544.
8 H. Lilja, A. Christensson, U. Dahlén, M. T. Matikainen, O. Nilsson, K. Pettersson and T. Lövgren, Prostate-specific antigen in serum occurs predominantly in complex with alpha 1-antichymotrypsin, *Clin. Chem.*, 1991, **37**, 1618–1625.
9 S. Raoofi Mohseni, F. Golsaz-Shirazi, M. Hosseini, J. Khoshnoodi, T. Bahadori, M. A. Judaki, M. Jeddi-Tehrani and F. Shokri, Characterization of Monoclonal and Polyclonal Antibodies Recognizing Prostate Specific Antigen: Implication for Design of a Sandwich ELISA, *Avicenna J. Med. Biotechnol.*, 2019, **11**, 72–79.
10 K. Jung, B. Brux, M. Lein, B. Rudolph, G. Kristiansen, S. Hauptmann, D. Schnorr, S. A. Loening and P. Sinha, Molecular Forms of Prostate-specific Antigen in Malignant and Benign Prostatic Tissue: Biochemical and Diagnostic Implications, *Clin. Chem.*, 2000, **46**, 47–54.
11 H. J. Linton, L. S. Marks, L. S. Millar, C. L. Knott, H. G. Rittenhouse and S. D. Mikolajczyk, Benign Prostate-specific Antigen (BPSA) in Serum Is Increased in Benign Prostate Disease, *Clin. Chem.*, 2003, **49**, 253–259.
12 L. I. Stowell, L. E. Sharman and K. Hamel, An enzyme-linked immunosorbent assay (ELISA) for prostate-specific antigen, *Forensic Sci. Int.*, 1991, **50**, 125–138.
13 J. Liang, C. Yao, X. Li, Z. Wu, C. Huang, Q. Fu, C. Lan, D. Cao and Y. Tang, Silver nanoprism etching-based plasmonic ELISA for the high sensitive detection of prostate-specific antigen, *Biosens. Bioelectron.*, 2015, **69**, 128–134.
14 S. Zhang, P. Du and F. Li, Detection of prostate specific antigen with 3,4-diaminobenzoic acid (DBA)–H2O2–HRP voltammetric enzyme-linked immunoassay system, *Talanta*, 2007, **72**, 1487–1493.
15 X.-H. Pham, E. Hahm, K.-H. Huynh, B. S. Son, H.-M. Kim and B.-H. Jun, Sensitive Colorimetric Detection of Prostate Specific Antigen Using a Peroxidase-Mimicking Anti-PSA Antibody Coated Au Nanoparticle, *BioChip J.*, 2020, **14**, 158–168.
16 N. Xia, D. Deng, Y. Wang, C. Fang and S.-J. Li, Gold nanoparticle-based colorimetric method for the detection of prostate-specific antigen, *Int. J. Nanomed.*, 2018, **13**, 2521–2530.
17 P.-Y. You, F.-C. Li, M.-H. Liu and Y.-H. Chan, Colorimetric and Fluorescent Dual-Mode Immunoassay Based on Plasmon-Enhanced Fluorescence of Polymer Dots for Detection of PSA in Whole Blood, *ACS Appl. Mater. Interfaces*, 2019, **11**, 9841–9849.
18 D. Damborska, T. Bertok, E. Dosekova, A. Holazova, L. Lorencova, P. Kasak and J. Tkac, Nanomaterial-based biosensors for detection of prostate specific antigen, *Microchim. Acta*, 2017, **184**, 3049–3067.
19 D. Wu, A. C. Sedgwick, T. Gunnlaugsson, E. U. Akkaya, J. Yoon and T. D. James, Fluorescent chemosensors: the past, present and future, *Chem. Soc. Rev.*, 2017, **46**, 7105–7123.
20 K. Kerman, T. Endo, M. Tsukamoto, M. Chikae, Y. Takamura and E. Tamiya, Quantum dot-based immunosensor for the detection of prostate-specific antigen using fluorescence microscopy, *Talanta*, 2007, **71**, 1494–1499.
21 Y. Chen, X. Guo, W. Liu and L. Zhang, Paper-based fluorometric immunodevice with quantum-dot labeled antibodies for simultaneous detection of carcinoembryonic antigen and prostate specific antigen, *Microchim. Acta*, 2019, **186**, 112.
22 M. K. Wagner, F. Li, J. Li, X.-F. Li and X. C. Le, Use of quantum dots in the development of assays for cancer biomarkers, *Anal. Bioanal. Chem.*, 2010, **397**, 3213–3224.

23 I. V. Koktysh, Y. I. Melnikova, O. S. Kulakovich, A. A. Ramanenka, S. V. Vaschenko, A. O. Muravitskaya, S. V. Gaponenko and S. A. Maskevich, Highly Sensitive Immunofluorescence Assay of Prostate-Specific Antigen Using Silver Nanoparticles, *J. Appl. Spectrosc.*, 2020, **87**, 870–876.

24 D. Liu, X. Huang, Z. Wang, A. Jin, X. Sun, L. Zhu, F. Wang, Y. Ma, G. Niu, A. R. Hight Walker and X. Chen, Gold Nanoparticle-Based Activatable Probe for Sensing Ultralow Levels of Prostate-Specific Antigen, *ACS Nano*, 2013, **7**, 5568–5576.

25 X. Li, L. Wei, L. Pan, Z. Yi, X. Wang, Z. Ye, L. Xiao, H.-W. Li and J. Wang, Homogeneous Immunosorbent Assay Based on Single-Particle Enumeration Using Upconversion Nanoparticles for the Sensitive Detection of Cancer Biomarkers, *Anal. Chem.*, 2018, **90**, 4807–4814.

26 H. M. E. Azzazy, M. M. H. Mansour and S. C. Kazmierczak, From diagnostics to therapy: Prospects of quantum dots, *Clin. Biochem.*, 2007, **40**, 917–927.

27 S. Veeranarayanan, A. Cheruvathoor Poulose, S. Mohamed, A. Aravind, Y. Nagaoka, Y. Yoshida, T. Maekawa and D. S. Kumar, FITC Labeled Silica Nanoparticles as Efficient Cell Tags: Uptake and Photostability Study in Endothelial Cells, *J. Fluoresc.*, 2012, **22**, 537–548.

28 V. Gubala, G. Giovannini, F. Kunc, M. P. Monopoli and C. J. Moore, Dye-doped silica nanoparticles: synthesis, surface chemistry and bioapplications, *Cancer Nanotechnol.*, 2020, **11**, 1–43.

29 I. Miletto, A. Gilardino, P. Zamburlin, S. Dalmazzo, D. Lovisolo, G. Caputo, G. Viscardi and G. Martra, Highly bright and photostable cyanine dye-doped silica nanoparticles for optical imaging: Photophysical characterization and cell tests, *Dyes Pigm.*, 2010, **84**, 121–127.

30 C. L. O'Connell, R. Nooney and C. McDonagh, Cyanine5-doped silica nanoparticles as ultra-bright immunospecific labels for model circulating tumour cells in flow cytometry and microscopy, *Biosens. Bioelectron.*, 2017, **91**, 190–198.

31 C.-J. Xie, D.-G. Yin, J. Li, L. Zhang, B.-H. Liu and M.-H. Wu, Preparation of A Novel Type of Fluorescein Isothiocyanate-Doped Fluorescent Silica Nanoparticle and Its Application as pH Probe, *Fenxi Huaxue*, 2010, **38**, 488–492.

32 P. D. K. P. Ananda, A. Tillekaratne, C. Hettiarachchi and N. Lalichchandran, Sensitive detection of E. coli using bioconjugated fluorescent silica nanoparticles, *Appl. Surf. Sci. Adv.*, 2021, **6**, 100159.

33 L. Min, L. Zhao-Yue, L. Qiang, Y. Hang, M. Lan, L. Jing-Hong, B. Yu-Bai and L. Tie-Jin, Functionalized Fluorescein-doped SiO2 Nanoparticles for Immunochromatographic Assay, *Chin. J. Chem.*, 2005, **23**, 875–880.

34 C. J. Moore, G. Giovannini, F. Kunc, A. J. Hall and V. Gubala, 'Overloading' fluorescent silica nanoparticles with dyes to improve biosensor performance, *J. Mater. Chem. B*, 2017, **5**, 5564–5572.

35 A. Van Blaaderen and A. Vrij, Synthesis and characterization of colloidal dispersions of fluorescent, monodisperse silica spheres, *Langmuir*, 1992, **8**, 2921–2931.

36 W. Wei, M. Wei and S. Liu, Silica nanoparticles as a carrier for signal amplification, *Rev. Anal. Chem.*, 2012, **31**, 163–176.

37 A. Auger, J. Samuel, O. Poncelet and O. Raccurt, A comparative study of non-covalent encapsulation methods for organic dyes into silica nanoparticles, *Nanoscale Res. Lett.*, 2011, **6**, 328.

38 G. Giovaninni, C. J. Moore, A. J. Hall, H. J. Byrne and V. Gubala, pH-Dependent silica nanoparticle dissolution and cargo release, *Colloids Surf., B*, 2018, **169**, 242–248.

39 O. K. Adeniyi, A. Ngqinambi and P. N. Mashazi, Ultrasensitive detection of anti-p53 autoantibodies based on nanomagnetic capture and separation with fluorescent sensing nanobioprobe for signal amplification, *Biosens. Bioelectron.*, 2020, **170**, 112640.

40 A. Shrivastava and V. Gupta, Methods for the determination of limit of detection and limit of quantitation of the analytical methods, *Chron. Young Sci.*, 2011, **2**, 21.

41 Z. Gao, M. Xu, L. Hou, G. Chen and D. Tang, Magnetic Bead-Based Reverse Colorimetric Immunoassay Strategy for Sensing Biomolecules, *Anal. Chem.*, 2013, **85**, 6945–6952.

42 L. Li, W. Zhang, Y. Wei, L. Yu and D. Feng, A Sensitive Fluorescent Immunoassay for Prostate Specific Antigen Detection Based on Signal Amplify Strategy of Horseradish Peroxidase and Silicon Dioxide Nanospheres, *J. Anal. Methods Chem.*, 2022, **2022**, 1–9.

43 Y. Zhao, W. Gao, X. Ge, S. Li, D. Du and H. Yang, CdTe@SiO2 signal reporters-based fluorescent immunosensor for quantitative detection of prostate specific antigen, *Anal. Chim. Acta*, 2019, **1057**, 44–50.

44 X. Wang, R. Xu, X. Sun, Y. Wang, X. Ren, B. Du, D. Wu and Q. Wei, Using reduced graphene oxide-Ca:CdSe nanocomposite to enhance photoelectrochemical activity of gold nanoparticles functionalized tungsten oxide for highly sensitive prostate specific antigen detection, *Biosens. Bioelectron.*, 2017, **96**, 239–245.

45 D. Mwanza, N. Mfamela, O. Adeniyi, T. Nyokong and P. Mashazi, Ultrasensitive detection of prostate-specific antigen using glucose-encapsulated nanoliposomes anti-PSA polyclonal antibody as detection nanobioprobes, *Talanta*, 2022, **245**, 123483.